JOURNAL OF GUIDANCE, CONTROL, AND DYNAMICS
Vol. 35, No. 2, March–April 2012

Analytical Nonlinear Propagation of Uncertainty in the Two-Body Problem

K. Fujimoto* and D. J. Scheeres†
University of Colorado at Boulder, Boulder, Colorado, 80309-0431
and
K. T. Alfriend‡
Texas A&M University, College Station, Texas, 77843-3141

DOI: 10.2514/1.54385

One topic of recent interest in the field of space situational awareness is the accurate and consistent representation of an observed object's uncertainty under nonlinear dynamics. This paper presents a method of analytical nonlinear propagation of uncertainty under two-body dynamics. In particular, the probability density function over state space and its mean and covariance matrix are expressed analytically for all time via a special solution of the Fokker-Planck equations for deterministic Hamiltonian systems. The state transition tensor concept is used to express the solution flow of the dynamics. Some numerical examples, where a second-order state transition tensor is found to sufficiently capture the nonlinear effects, are also discussed.

I. Introduction

SITUATIONAL awareness of Earth-orbiting particles, such as active satellites and space debris, is highly important for all current and future space-faring nations. One topic of recent interest is the accurate and consistent representation of an observed object's uncertainty under nonlinear dynamics [1,2]. Traditional orbit-estimation methods rely on linear propagation of Gaussian uncertainty [3]. It has been shown, however, that the Gaussian assumption is an inconsistent description of the actual uncertainty when the dynamics are highly unstable or when propagation times become long [2,4–6]. Several methods have been proposed to incorporate the nonlinearity of the dynamics of objects in orbit and to express the non-Gaussianity of the resulting probability distribution, including Gaussian sums, Monte Carlo simulations, and Edgeworth filters [1,2,7]. The problem with the aforementioned approaches is that they require significant computational power.

This paper is a survey of analytical nonlinear propagation of uncertainty under two-body dynamics in the Poincaré orbit element space. In particular, ways to express, analytically and for all time, the probability density function (PDF) over Poincaré space and its mean and covariance matrix are presented. This theory will allow one to, for example, improve the accuracy and computational turnaround of the correlation of optical tracks and initial orbit determination using the admissible region concept [8–10]. First, the necessary mathematical and physical ideas (section II) are introduced. For a deterministic Hamiltonian dynamical system, as long as one has an analytical description of the initial PDF and the solution to the dynamics, an analytical description of the PDF for all time can be obtained [4]. Given an analytical expression of the PDF, time propagation is extremely efficient, as it is only a matter of changing the time parameter. One way to express the solution of the dynamics is via state transition tensors (STTs) [4,11]. Then, the preceding ideas are applied to the orbiter problem (section III). A closed-form STT solution for the two-body problem and the two-body problem with perturbations from J_2 gravity field harmonics in the Poincaré orbit element space are presented. These dynamical systems are chosen for consideration in the current paper because their solution flow is analytical, but more complex systems can be accounted for. Finally, some numerical examples are discussed (section IV). The mean and covariance matrix of a PDF, as well as its 3-σ ellipse, propagated using STTs and those calculated via Monte Carlo methods are compared. Also, the prediction error metric as defined by Horwood et al. [2] is computed to determine how well the proposed method maintains uncertainty consistency. Overall, this method succeeds in accurately propagating uncertainty without excessive computational burden.

II. Background

In this section, the concepts and theories that are used in this paper are introduced. Mainly, the solutions to the Fokker-Planck equation for a deterministic Hamiltonian (i.e., nondissipative) system and the nonlinear mapping of both the system state and the moments/cumulants of a PDF using the STT are discussed.

A. Solution of the Fokker-Planck Equation For a Deterministic Hamiltonian System

Suppose the dynamics of some system is expressed as

$$\dot{\mathbf{X}} = \boldsymbol{f}(t, \mathbf{X}) \tag{1}$$

where $\mathbf{X}$ is the state vector, and $\boldsymbol{f}$ are the equations of motion [4]. Then, the solution of Eq. (1) is expressed as

$$\mathbf{X}(t) = \boldsymbol{\phi}(t; \mathbf{X}^0, t^0) \tag{2}$$

where $\mathbf{X}^0$ is the initial state at time t^0. $\boldsymbol{\phi}$ must satisfy the following conditions:

$$\frac{\mathrm{d}\boldsymbol{\phi}}{\mathrm{d}t} = \boldsymbol{f}(t, \boldsymbol{\phi}(t; \mathbf{X}^0, t)) \tag{3}$$

and

$$\boldsymbol{\phi}(t^0; \mathbf{X}^0, t^0) = \mathbf{X}^0 \tag{4}$$

The inverse solution flow $\boldsymbol{\psi}(t, \mathbf{X}; t^0)$ is defined as

Received 28 March 2011; revision received 24 July 2011; accepted for publication 27 July 2011.

*Graduate Student, Department of Aerospace Engineering Sciences, 431 UCB 166 ECEE; kohei.fujimoto@colorado.edu. Member AIAA (Corresponding Author).

†A. Richard Seebass Chair, Department of Aerospace Engineering Sciences, 429 UCB ECOT 611. Fellow AIAA.

‡TEES Distinguished Research Chair Professor, Department of Aerospace Engineering, H.R. Bright Building, Room 701, 3141 TAMU. Fellow AIAA.

$$\mathbf{X}^0 = \boldsymbol{\psi}(t, \mathbf{X}; t^0) \tag{5}$$

which maps a current state back to an earlier state. Technically, for a general solution to the flow, this flow can be found by interchanging the initial and final states

$$\boldsymbol{\psi}(t, \mathbf{X}; t^0) = \boldsymbol{\phi}(t^0; \mathbf{X}, t) \tag{6}$$

For a system that satisfies the Itô stochastic differential equation, the time evolution of a PDF, $p(\mathbf{X}, t)$, over $\mathbf{X}$ at time, t, is described by the Fokker-Planck equation [7]

$$\frac{\partial p(\mathbf{X}, t)}{\partial t} = -\sum_{i=1}^{n} \frac{\partial}{\partial \mathbf{X}_i}\{p(\mathbf{X}, t)\boldsymbol{f}_i(\mathbf{X}, t)\} + \frac{1}{2}\sum_{i=1}^{n}\sum_{j=1}^{n} \frac{\partial^2}{\partial \mathbf{X}_i \partial \mathbf{X}_j}[p(\mathbf{X}, t)\{G(\mathbf{X}, t)Q(t)G^T(\mathbf{X}, t)\}_{ij}] \tag{7}$$

where a single subscript indicates vector components, and a double subscript indicates matrix components. Matrices G and Q characterize the diffusion. For a deterministic Hamiltonian system, a special solution of Eq. (7) exists, and it can be shown that the total time derivative of a PDF is zero, independent of whether the potential field is time invariant [4]. Thus, the PDF, $p[\mathbf{X}(t)]$, is a constant and can be expressed in terms of the initial conditions, t^0 and $\mathbf{X}^0$, as

$$p[\boldsymbol{\phi}(t; \mathbf{X}^0, t^0)] = p[\mathbf{X}(t)] = p(\mathbf{X}^0) = p[\boldsymbol{\psi}(t, \mathbf{X}; t^0)] \tag{8}$$

That is, if one has analytical expressions for the initial PDF and the solution flow, $\boldsymbol{\phi}(t; \mathbf{X}^0, t^0)$, for all t, then the analytical expression for the PDF can be obtained for all t. Analytical expressions of the PDF are useful because propagation is then only a matter of changing the value for t. In particular, if the initial PDF is an n-dimensional Gaussian distribution,

$$p(\mathbf{X}^0) = \frac{1}{\sqrt{(2\pi)^{2n}|[P^0]|}} \exp\left\{\frac{1}{2}(\mathbf{X}^0 - \mathbf{M}^0)^T[P^0]^{-1}(\mathbf{X}^0 - \mathbf{M}^0)\right\} \tag{9}$$

where the brackets indicate a matrix, superscript -1 indicates an inverse, vertical lines represent the determinant, $\mathbf{M}^0$ is the initial mean of the Gaussian, and $[P^0]$ is the initial covariance matrix. Then, the PDF at time t is

$$p[\mathbf{X}(t)] = \frac{1}{\sqrt{(2\pi)^{2n}|[P^0]|}} \exp\left\{\frac{1}{2}(\boldsymbol{\psi}(t, \mathbf{X}; t^0) - \mathbf{M}^0)^T \times [P^0]^{-1}(\boldsymbol{\psi}(t, \mathbf{X}; t^0) - \mathbf{M}^0)\right\} \tag{10}$$

because $\mathbf{M}^0$ and $[P^0]$ are initial parameters of the system and are constants.

As a consequence of Eq. (8), the probability is an integral invariant

$$\int_{\mathcal{B}} p[\mathbf{X}(t)]\,\mathrm{d}\mathbf{X} = \int_{\mathcal{B}^0} p(\mathbf{X}^0)\,\mathrm{d}\mathbf{X}^0 \tag{11}$$

where $\mathbf{X} \in \mathcal{B}$, and $\mathcal{B}^0$ is the corresponding region for $\mathbf{X}^0 = \boldsymbol{\psi}(t, \mathbf{X}; t^0)$ [12,13].

B. Prediction Error as an Uncertainty Consistency Metric

In a classical approach to statistical orbit determination, such as the Kalman filter, uncertainty is modeled as a Gaussian distribution and is propagated linearly about a reference trajectory [3]. The mean of the state deviation, if assumed to be on the reference orbit, is zero for all time, and the covariance matrix, $[P](t)$, is propagated with the state transition matrix, $[\Phi](t, t^0)$,

$$[P](t) = [\Phi](t, t^0) \circ [P^0] \circ [\Phi]^T(t, t^0) \tag{12}$$

All higher-order moments and cumulants are zero for all time. Although this approach is mathematically well-studied and easy to implement, the assumption that the dynamics are linear has been shown to break down even after one orbit for an object in low-Earth orbit, depending on the coordinate system used [5,6]. The propagated uncertainty is then no longer an "accurate reflection of the discrepancy from truth exhibited by an estimated state" [2] due to the nonlinearity of the dynamics [4]. That is, the uncertainty is inconsistent.

To distinguish the validity of various linear and nonlinear uncertainty propagation techniques, Horwood, et al. [2] have proposed a simple online uncertainty consistency metric called the prediction error, $\mathcal{PE}(t)$, which is defined as follows:

$$\mathcal{PE}(t) = \int p_1[\mathbf{X}(t)]p_2[\mathbf{X}(t)]\,\mathrm{d}\mathbf{X} \tag{13}$$

where p_1 and p_2 are two arbitrary PDFs, and the integration is over the entire state space. Again, from Eq. (8), $\mathcal{PE}(t)$ should be time-independent assuming a deterministic Hamiltonian dynamical system and consistent uncertainty propagation. In section IV.C, this metric is used to quantify the consistency of uncertainty propagation for the proposed method using solutions to the Fokker-Planck equation versus the classical linear propagation.

C. Non-Linear Mapping of System Dynamics using State Transition Tensors

One method of obtaining an analytical, nonlinear approximation to the solution flow, $\boldsymbol{\phi}(t; \mathbf{X}^0, t^0)$, is to use a concept called the STT. If one takes a Taylor series expansion of the solution function Eq. (2) about some reference trajectory, $\mathbf{X}^*$, the state deviation, $\mathbf{x} = \mathbf{X} - \mathbf{X}^*$, is found as

$$\mathbf{x}_i(t) = \sum_{p=1}^{m} \frac{1}{p!} \Phi_{i,k_1\ldots k_p} \mathbf{x}^0_{k_1} \ldots \mathbf{x}^0_{k_p} \tag{14}$$

where the subscripts indicate the component of each tensor, m is the order of the expansion, and Φ is the STT of order p [4,11]. Einstein's summation notation is used, and the comma in the subscript simply denotes that the i-th component is not summed over. Note that the STT is a generalization of the state transition matrix (STM) to any arbitrary order. For $m = 1$, one finds the familiar result

$$\mathbf{x}_i(t) = \Phi_{i,k_1}\mathbf{x}^0_{k_1} \Rightarrow \mathbf{x}(t) = [\Phi]\mathbf{x}^0 \tag{15}$$

Given the solution flow, $\boldsymbol{\phi}$, the STT can be solved for

$$\Phi_{i,k_1\ldots k_p} = \left.\frac{\partial^p \mathbf{X}_i}{\partial \mathbf{X}^0_{k_1} \ldots \partial \mathbf{X}^0_{k_p}}\right|_* \tag{16}$$

where the * indicates that Φ is evaluated over the reference trajectory $\mathbf{X}^*$. If $\mathbf{X}$ is not given as a function of $\mathbf{X}^0$, then the following differential equation is solved:

$$\dot{\Phi}_{i,k_1\ldots k_p} = G(A_{i,k_1}, \ldots, A_{i,k_1\ldots k_p}; \Phi_{i,k_1}, \ldots, \Phi_{i,k_1\ldots k_p}) \tag{17}$$

where

$$A_{i,k_1\ldots k_p} = \left.\frac{\partial^p \boldsymbol{f}_i}{\partial \mathbf{X}_{k_1} \ldots \mathbf{X}_{k_p}}\right|_* \tag{18}$$

is the local dynamics tensor (LDT), and G is a function described as follows. Each term in G is a product of an LDT and STTs so that 1) the sum of the orders of the STTs add up to p and 2) the number of STTs in the term is equal to the order of the LDT.

For instance, for $p = 5$, terms of the form

1) $A_{i,l_1}\Phi_{l_1,k_1k_2k_3k_4k_5}\ \langle 1\rangle$;

2) $A_{i,l_1l_2}\Phi_{l_1,k_1k_2k_3k_4}\Phi_{l_2,k_5}\ \langle 5\rangle$, $A_{i,l_1l_2}\Phi_{l_1,k_1k_2k_3}\Phi_{l_2,k_4k_5}\ \langle 10\rangle$;

3) $A_{i,l_1l_2l_3}\Phi_{l_1,k_1}\Phi_{l_2,k_2}\Phi_{l_3,k_3k_4k_5}\ \langle 10\rangle$, $A_{i,l_1l_2l_3}\Phi_{l_1,k_1}\Phi_{l_2,k_2k_3}\Phi_{l_3,k_4k_5}\ \langle 15\rangle$;

4) $A_{i,l_1l_2l_3l_4}\Phi_{l_1,k_1}\Phi_{l_2,k_2}\Phi_{l_3,k_3}\Phi_{l_4,k_4k_5}\ \langle 10\rangle$; and

5) $A_{i,l_1l_2l_3l_4l_5}\Phi_{l_1,k_1}\Phi_{l_2,k_2}\Phi_{l_3,k_3}\Phi_{l_4,k_4}\Phi_{l_5,k_5}\ \langle 1\rangle$

appear, where the number in $\langle\cdot\rangle$ is the number for permutations of $k_1, \ldots, k_p$ that exist, e.g., for $A_{i,l_1l_2}\Phi_{l_1,k_1k_2k_3k_4}\Phi_{l_2,k_5}$

$$A_{i,l_1l_2}\Phi_{l_1,k_2k_3k_4k_5}\Phi_{l_2,k_1}, A_{i,l_1l_2}\Phi_{l_1,k_1k_3k_4k_5}\Phi_{l_2,k_2}, A_{i,l_1l_2}\Phi_{l_1,k_1k_2k_4k_5} \times \Phi_{l_2,k_3}, A_{i,l_1l_2}\Phi_{l_1,k_1k_2k_3k_5}\Phi_{l_2,k_4}, A_{i,l_1l_2}\Phi_{l_1,k_1k_2k_3k_4}\Phi_{l_2,k_5} \tag{19}$$

G is the sum of all possible forms and permutations mentioned in the preceding list. Again, for $n = 5$,

$$\begin{aligned} G(A_{i,k_1},\ldots,A_{i,k_1k_2k_3k_4k_5};\Phi_{i,k_1},\ldots,\Phi_{i,k_1k_2k_3k_4k_5}) &= A_{i,l_1}\Phi_{l_1,k_1k_2k_3k_4k_5} \\ &+ A_{i,l_1l_2}\Phi_{l_1,k_2k_3k_4k_5}\Phi_{l_2,k_1} + A_{i,l_1l_2}\Phi_{l_1,k_1k_3k_4k_5}\Phi_{l_2,k_2} \\ &+ A_{i,l_1l_2}\Phi_{l_1,k_1k_2k_4k_5}\Phi_{l_2,k_3} + A_{i,l_1l_2}\Phi_{l_1,k_1k_2k_3k_5}\Phi_{l_2,k_4} \\ &+ A_{i,l_1l_2}\Phi_{l_1,k_1k_2k_3k_4}\Phi_{l_2,k_5} + A_{i,l_1l_2}\Phi_{l_1,k_1k_2k_3}\Phi_{l_2,k_4k_5} + \ldots \\ &+ A_{i,l_1l_2l_3}\Phi_{l_1,k_1}\Phi_{l_2,k_2}\Phi_{l_3,k_3k_4k_5} + \ldots \\ &+ A_{i,l_1l_2l_3}\Phi_{l_1,k_1}\Phi_{l_2,k_2k_3}\Phi_{l_3,k_4k_5} + \ldots \\ &+ A_{i,l_1l_2l_3l_4}\Phi_{l_1,k_1}\Phi_{l_2,k_2}\Phi_{l_3,k_3}\Phi_{l_4,k_4k_5} + \ldots \\ &+ A_{i,l_1l_2l_3l_4l_5}\Phi_{l_1,k_1}\Phi_{l_2,k_2}\Phi_{l_3,k_3}\Phi_{l_4,k_4}\Phi_{l_5,k_5} \end{aligned} \tag{20}$$

The initial values for the integration of Eq. (17) are $\Phi_{i,a} = 1$ for $i = a$ and 0 for all other entries. A and G are the generalization of the linear dynamics matrix to any arbitrary order. Again, when $m = 1$, one finds the familiar result

$$\dot{\Phi}_{i,k_1} = A_{i,l_1}\Phi_{l_1,k_1} \Rightarrow [\dot{\Phi}] = [A][\Phi] \tag{21}$$

D. Non-Linear Mapping of the Mean and Covariance Matrix of the PDF

In some cases, it is more useful to obtain an analytical approximation to the mean, $\mathbf{M} = \mathbf{m} + \mathbf{X}^*$, and covariance matrix, $[P]$, of the PDF, $p[\mathbf{X}(t)]$, rather than the PDF itself. Given some initial state deviation, $\mathbf{x}^0$, at time, t^0,

$$\mathbf{m}_i(t) = \sum_{p=1}^{m} \frac{1}{p!}\Phi_{i,k_1\ldots k_p}E[\mathbf{x}^0_{k_1}\ldots\mathbf{x}^0_{k_p}] \tag{22}$$

$$[P]_{ij}(t) = \left(\sum_{p=1}^{m}\sum_{q=1}^{m}\frac{1}{p!q!}\Phi_{i,k_1\ldots k_p}\Phi_{j,l_1\ldots l_q}E[\mathbf{x}^0_{k_1}\ldots\mathbf{x}^0_{k_p}\mathbf{x}^0_{l_1}\ldots\mathbf{x}^0_{l_q}]\right) - \mathbf{m}_i(t)\mathbf{m}_j(t) \tag{23}$$

where m is the order of the expansion of the dynamics, and E is the expected value operator as defined in Park and Scheeres [4]

$$E[f(\mathbf{x})] = \int_{\infty} f(\mathbf{x})p[\mathbf{x}(t)]\,\mathrm{d}\mathbf{x} \tag{24}$$

Up to an $2m$-order moment of the initial PDF is required to propagate the covariance matrix, where an n-th-order moment, $\kappa^{i_1\ldots i_n}$, is defined in Horwood [1] and McCullaugh [14] as

$$\kappa^{i_1\ldots i_n} = E[\mathbf{x}_{i_1}\ldots\mathbf{x}_{i_n}] \tag{25}$$

Thus, even for a fourth-order dynamics expansion, to propagate the covariance matrix, one requires up to an eighth-order moment, which for a six-dimensional state space, is composed of $6^8 \approx 10^6$ terms. Memory burden may be reduced by exploiting the fact that the moment is a symmetric tensor. Another useful property to speed up computation is as follows. Also define an n-th-order cumulant, $\kappa^{i_1,\ldots,i_n}$, as

$$\kappa^{i_1,\ldots,i_n} = E[(\mathbf{x}_{i_1} - \mathbf{m}_{i_1})\ldots(\mathbf{x}_{i_n} - \mathbf{m}_{i_n})] \tag{26}$$

Then, the n-th-order moment can be expressed in terms of cumulants of order up to n

$$\kappa^{i_1\ldots i_n} = H(\kappa^{i_1},\ldots,\kappa^{i_1,\ldots,i_n}) \tag{27}$$

where H is a function defined similar to the function G of the differential equations of the STT. That is, each term in H is a product of the cumulants such that the sum of their orders add up to n. H is the sum of all possible forms and permutations of such terms. For an initial Gaussian distribution, many terms in H drop out as all cumulants of order 3 and greater are 0. In fact, for such a case, an n-th-order moment can be expressed entirely in terms of the mean and covariance matrix. Despite this simplification, to propagate such a higher-order moment still requires high-rank STTs, which act as a computational block to describing a PDF in terms of its moments. It must be emphasized that, with this formulation, it is not necessary to compute these higher-order moments to determine the PDF at some future time. Rather, computation of these moments is restricted to situations in which they convey some specific meaning or have some specific use, such as initialization of an orbit determination algorithm.

III. Method

Motion of satellites in Earth orbit are particularly amenable to having their solution described through analytic or semi-analytic techniques. Even when stronger nongravitational perturbations, such as solar radiation pressure and atmospheric drag, are encountered, these perturbations generally have deterministic components that are substantially larger than their time-varying stochastic components, meaning that they can be modeled either numerically or, in some cases, analytically. These facts open the door to the use and application of analytical or semi-analytical techniques to describe the motion of a satellite, even accounting for uncertainty in model parameters, so long as they do not contain strong dynamical stochastic variations. In particular, if an approximate technique is found for describing the dynamics of a satellite over time, such a solution can be applied to a range of important questions related to the dynamical propagation of an object's PDF.

One such question is the propagation of range/range-rate uncertainties associated with an optical track of an Earth-orbiting object (i.e., the admissible region) [8,9] Multiple admissible regions may be mapped to a common epoch and combined by means of Bayes' theorem to correlate optical tracks and obtain an initial orbit estimate [10]. Currently, this mapping is done by dividing up the admissible region into smaller subsets and propagating them linearly. With a nonlinear propagation technique, better accuracy and faster computational turnaround are expected because one can robustly propagate larger subregions.

To this end, in this section, the STTs for two-body dynamics and two-body dynamics with J_2 gravity field perturbations are explicitly derived. Although it has been indicated in the preceding section how this approach can be applied to general and fully perturbed dynamical systems, in the current paper, it is applied only to systems with analytical solution flows in order to simplify the math considerably. Thus, the secular J_2 effects were chosen just as an example; it is possible to consider higher-order harmonics via methods by Brouwer[15], for instance.

A. Computation of n-th-Order STTs For Two-Body Dynamics

In two-body dynamics, the solution flow, $\boldsymbol{\phi}(t;\mathbf{X}^0,t^0)$, is given analytically

$$\begin{aligned} &\mathfrak{L}(t) = \mathfrak{L}^0 \qquad \mathfrak{l}(t) = \mathfrak{l}^0 + \mu^2/(\mathfrak{L}^0)^3(t-t^0) \qquad \mathfrak{G}(t) = \mathfrak{G}^0 \\ &\mathfrak{g}(t) = \mathfrak{g}^0 \qquad \mathfrak{H}(t) = \mathfrak{H}^0 \qquad \mathfrak{h}(t) = \mathfrak{h}^0 \end{aligned} \tag{28}$$

where μ is the standard gravitational parameter and $\mathbf{X}(t) = (\mathfrak{L}(t), \mathfrak{l}(t), \mathfrak{G}(t), \mathfrak{g}(t), \mathfrak{H}(t), \mathfrak{h}(t))$ are the Poincaré orbit elements [16]. The Poincaré orbit elements are the nonsingular canonical counterpart to the equinoctial orbit elements. Their main advantage is that the variables can be naturally grouped into coordinate-momenta symplectic pairs. Furthermore, they are defined and nonsingular even for circular and zero-inclination orbits. With respect to the classical orbital elements

$$\mathfrak{L} = \sqrt{\mu a} \qquad \mathfrak{l} = \Omega + \omega + M$$
$$\mathfrak{G} = -\mathfrak{g}\tan(\omega+\Omega) \qquad \mathfrak{g} = \sqrt{2\mathfrak{L}(1-\sqrt{1-e^2})}\cos(\omega+\Omega)$$
$$\mathfrak{H} = -\mathfrak{h}\tan\Omega \qquad \mathfrak{h} = \sqrt{2\mathfrak{L}\sqrt{1-e^2}(1-\cos i)}\cos\Omega \tag{29}$$

where a is the semimajor axis, e is the eccentricity, i is the inclination, Ω is the right acsension of the ascending node, ω is the argument of periapsis, and M is the mean anomaly. The inverse transformation, $\boldsymbol{\psi}(t, \mathbf{X}; t^0)$, is

$$\mathfrak{L}^0(t) = \mathfrak{L} \qquad \mathfrak{l}^0(t) = \mathfrak{l} + \mu^2/\mathfrak{L}^3(t^0 - t)$$
$$\mathfrak{G}^0(t) = \mathfrak{G} \qquad \mathfrak{g}^0(t) = \mathfrak{g}$$
$$\mathfrak{H}^0(t) = \mathfrak{H} \qquad \mathfrak{h}^0(t) = \mathfrak{h} \tag{30}$$

From Eq. (28), Φ is expected to be very sparse, as derivatives higher than and including second-order for all variables except $\mathfrak{l}$ are 0

$$\Phi_{i,k_1\ldots k_p} = \begin{cases} [(-1)^p\mu^2(p+2)!\Delta t/2!]/[(\mathfrak{L}^0)^{p+3}] & i=2 \quad \text{and} \quad k_1=k_2=\ldots=k_p=1 \\ 1 & p=1 \quad \text{and} \quad k_1=i \\ 0 & \text{elsewhere} \end{cases} \tag{31}$$

where $\Delta t = t - t^0$ is the time duration of the propagation. Similarly, the STT Ψ of order p corresponding to the inverse flow is simply

$$\Psi_{i,k_1\ldots k_p} = \begin{cases} [(-1)^p\mu^2(p+2)!(-\Delta t)/2!]/[(\mathfrak{L})^{p+3}] & i=2 \quad \text{and} \quad k_1=k_2=\ldots=k_p=1 \\ 1 & p=1 \quad \text{and} \quad k_1=i \\ 0 & \text{elsewhere} \end{cases} \tag{32}$$

B. Computation of n-th-Order STTs For Two-Body Dynamics+Averaged J_2 Perturbations

The effects of the averaged (or secular) J_2 gravity field perturbations are now added to the preceding two-body STT. In classical orbital elements, the results are well known, as presented in Vallado [16],

$$\dot{a}_{\text{sec}} = 0 \qquad \dot{\Omega}_{\text{sec}} = -\frac{3n^0 r_E^2 J_2}{2(p^0)^2}\cos i^0 \qquad \dot{e}_{\text{sec}} = 0$$
$$\dot{\omega}_{\text{sec}} = \frac{3n^0 r_E^2 J_2}{4(p^0)^2}(4 - 5\sin^2 i^0) \qquad \dot{i}_{\text{sec}} = 0$$
$$\dot{M}^0_{\text{sec}} = \frac{-3n^0 r_E J_2\sqrt{1-(e^0)^2}}{4(p^0)^2}(3\sin^2 i^0 - 2) \tag{33}$$

where $n^0 = \sqrt{\mu/(a^0)^3}$ is the mean motion, r_E is the radius of the Earth, $p = a^0(1-(e^0)^2)$ is the semiparameter, and M^0 is the mean anomaly at epoch. The superscripts "0" are to emphasize that the preceding rates are all constant given initial conditions. Therefore,

$$a(t) = a^0 \qquad \Omega(t) = \Omega^0 + \dot{\Omega}_{\text{sec}}\Delta t \qquad e(t) = e^0$$
$$\omega(t) = \omega^0 + \dot{\omega}_{\text{sec}}\Delta t \qquad i(t) = i^0$$
$$M(t) = M^0 + (n^0 + \dot{M}^0_{\text{sec}})\Delta t \tag{34}$$

These relationships must be translated to Poincaré orbit elements. To do so, the Delaunay orbit elements, (L, l, G, g, H, h), are introduced. With respect to the classical orbit elements, they are defined by Vallado [16] as follows:

$$L = \sqrt{\mu a} \qquad l = M$$
$$G = L\sqrt{1-e^2} \qquad g = \omega$$
$$H = G\cos i \qquad h = \Omega \tag{35}$$

and with respect to the Poincaré orbit elements

$$L = \mathfrak{L} \qquad l = \mathfrak{l} + \arctan(\mathfrak{G}/\mathfrak{g})$$
$$G = \mathfrak{L} - \frac{\mathfrak{G}^2+\mathfrak{g}^2}{2} \qquad g = \arctan(\mathfrak{H}/\mathfrak{h}) - \arctan(\mathfrak{G}/\mathfrak{g})$$
$$H = \mathfrak{L} - \frac{\mathfrak{G}^2+\mathfrak{g}^2+\mathfrak{H}^2+\mathfrak{h}^2}{2} \qquad h = -\arctan(\mathfrak{H}/\mathfrak{h}) \tag{36}$$

For just this section, the state expressed in Delaunay elements is explicitly denoted as ${}^D\mathbf{X}(t)$, in Poincaré elements as ${}^P\mathbf{X}(t)$, and their initial states as ${}^D\mathbf{X}^0$ and ${}^P\mathbf{X}^0$, respectively. The goal in this section, then, is to find ${}^P\mathbf{X}(t)$ as a function of ${}^P\mathbf{X}^0$. Equation (34) is transformed into Delaunay orbit elements, presented by Maruskin et al. [8] as

$$L(t) = L^0 \qquad l(t) = l^0 + \left[\frac{-3\mu^4 r_E^2 J_2\{(G^0)^2 - 3(H^0)^2\}}{4(L^0)^4(G^0)^5} + \frac{\mu^2}{(L^0)^3}\right]\Delta t$$
$$G(t) = G^0 \qquad g(t) = g^0 + \left\{\frac{-3\mu^4 r_E^2 J_2}{4(L^0)^3(G^0)^4} + \frac{15\mu^4 r_E^2 J_2(H^0)^2}{4(L^0)^3(G^0)^6}\right\}\Delta t$$
$$H(t) = H^0 \qquad h(t) = h^0 - \frac{3\mu^4 r_E^2 J_2 H^0}{2(L^0)^3(G^0)^5}\Delta t \tag{37}$$

At this point, substitute Eq. (37) into the inverse relationship of Eq. (36)

$$\mathfrak{L} = L \qquad \mathfrak{l} = l + g + h$$
$$\mathfrak{G} = -\mathfrak{g}\tan(h+g) \qquad \mathfrak{g} = \sqrt{2(L-G)}\cos(h+g)$$
$$\mathfrak{H} = -\mathfrak{h}\tan(h) \qquad \mathfrak{h} = \sqrt{2(G-H)}\cos(h) \tag{38}$$

and further express ${}^D\mathbf{X}^0$ in terms of ${}^P\mathbf{X}^0$ via Eq. (36) to obtain ${}^P\mathbf{X}(t)$ as a function of ${}^P\mathbf{X}^0$. Then, calculating the STTs is, albeit tedious, algebraic work.

As will be seen in section IV.A, the averaged perturbation due to J_2 is dynamically slow enough compared with the two-body acceleration such that a first-order approximation (i.e., STM) of the perturbing dynamics is often sufficient to consistently propagate uncertainty. In such a case, a simpler way to compute the STM is to use the chain rule of differentiation

$$\frac{\partial^P\mathbf{X}(t)}{\partial^P\mathbf{X}^0} = \left(\frac{\partial^P\mathbf{X}(t)}{\partial^D\mathbf{X}(t)}\right)\circ\left(\frac{\partial^D\mathbf{X}(t)}{\partial^D\mathbf{X}^0}\right)\circ\left(\frac{\partial^D\mathbf{X}^0}{\partial^P\mathbf{X}^0}\right) \tag{39}$$

The first Jacobian matrix is a direct consequence of Eq. (38), the second matrix of Eq. (37), and the third of Eq. (36). The resulting STM does not contain any singularities; refer to appendix A for details. Again, for the higher-order STTs, it is assumed that

contributions from the averaged J_2 accelerations can be ignored; simply use the two-body solution as in Eq. (31).

IV. Results

In this section, results from C++ and MATLAB implementations of the theory discussed so far are presented. Unless otherwise stated, length units for all examples are in Earth radii, and all times are in units in hours.

A. Propagation of the 3-σ Ellipse

Here, a demonstration of how the 3-σ ellipse of an initial Gaussian distribution propagates under two-body dynamics and J_2 gravity field effects is shown. Results from the STT method and Monte Carlo simulations are compared.

1. *Two-body Dynamics*

For this example, the classical and Poincaré orbital elements of the truth orbit is given as follows:

$$a = 1.09437, \qquad e = i = \Omega = \omega = M = 0$$
$$\Rightarrow \mathfrak{L} = 4.6679 \qquad \mathfrak{l} = \mathfrak{G} = \mathfrak{g} = \mathfrak{H} = \mathfrak{h} = 0 \tag{40}$$

The orbit period is 1.6121 hrs. For this analysis, only the $\delta\mathfrak{L}$-$\delta\mathfrak{l}$ subspace is considered, where δ denotes state deviation from the reference because only $\mathfrak{l}$ dynamically evolves in the two-body problem, and its rate is a function of $\mathfrak{L}$. The initial Gaussian uncertainty is zero-mean, and two cases 1 and 2 of initial covariance matrices are considered

$$\text{(case 1) } [P] = \begin{bmatrix} \sigma_{\mathfrak{L}}^2 & \mu_{\mathfrak{L}\mathfrak{l}} \\ \mu_{\mathfrak{L}\mathfrak{l}} & \sigma_{\mathfrak{l}}^2 \end{bmatrix} = \begin{bmatrix} 4.4723 \times 10^{-5} & 0 \\ 0 & 3.0461 \times 10^{-8} \end{bmatrix} \tag{41}$$

$$\text{(case 2) } [P] = \begin{bmatrix} 0.06243 & 0 \\ 0 & 3.0461 \times 10^{-8} \end{bmatrix} \tag{42}$$

The corresponding 1-σ uncertainty in the semimajor axis direction is 20 km for case 1 and 745 km for case 2. Both cases 1 and 2 correspond to a 0.01 ° uncertainty in the mean longitude. Although case 2 is unrealistic, it will be used to show the robustness of the proposed method as well as to provide numerical stability in section iv.B. For the Monte Carlo simulation, 10^6 points distributed to be consistent with the initial uncertainty are generated and propagated using the complete two-body dynamics as in Eq. (28). For the STT propagation, 10^3 points are taken on the initial 3-σ ellipse and propagated using the approximate two-body dynamics as in Eq. (31). Figure 1 is a representation of these initial distributions.

Figures 2 and 3 shows the results of the propagation for case 1. From Eq. (8), the propagated 3-σ ellipses are expected to still enclose a large number of the propagated Monte Carlo sample points. Indeed, as the order of the STT used increases, the uncertainty map converges to the Monte Carlo solution. The 3-σ ellipse propagated with first-order dynamics encloses a small portion of the Monte Carlo points, whereas those propagated with higher-order STTs continue to enclose a majority. By about second-order, the STT approximation is close enough to the full dynamics. Also, the nonlinearity grows as the propagation time is made longer, as expected. Figure 3 is a representation of the Monte Carlo results and the propagated 3-σ ellipses after 100 orbital periods or about 161 hrs. The second-order and higher STTs continue to be sufficient approximations to the complete two-body dynamics even after such long propagation times.

Figure 4 shows the results of the propagation for case 2. Even for such an extreme initial distribution with faster dynamics, the STT propagation, particularly above third-order, continues to retain uncertainty consistency after ~161 hrs.. It is also more clear for this case how the expansion of the dynamics converges upon the true dynamics as one includes higher-order effects.

2. *Averaged J_2 Perturbations*

For this example, the classical and Poincaré orbital elements of the truth orbit is given as follows:

$$a = 1.09437, \qquad e = 0.1, \qquad i = \pi/6$$
$$\Omega = \pi/4, \qquad \omega = \pi/3, \qquad M = \pi/2 \tag{43}$$

$$\Rightarrow \mathfrak{L} = 4.6679, \qquad \mathfrak{l} = 3.4034, \qquad \mathfrak{G} = -0.20895$$
$$\mathfrak{g} = -0.055989, \qquad \mathfrak{H} = -0.78882, \qquad \mathfrak{h} = 0.78882 \tag{44}$$

The orbit period is still 1.6121 hrs. The analysis must be conducted in the full six-dimensional state space now, because all Poincaré elements except $\mathfrak{L}$ are functions of time. The initial Gaussian uncertainty is defined in the classical orbit element space and mapped into the Poincaré space. The mean is zero and the covariance matrix is

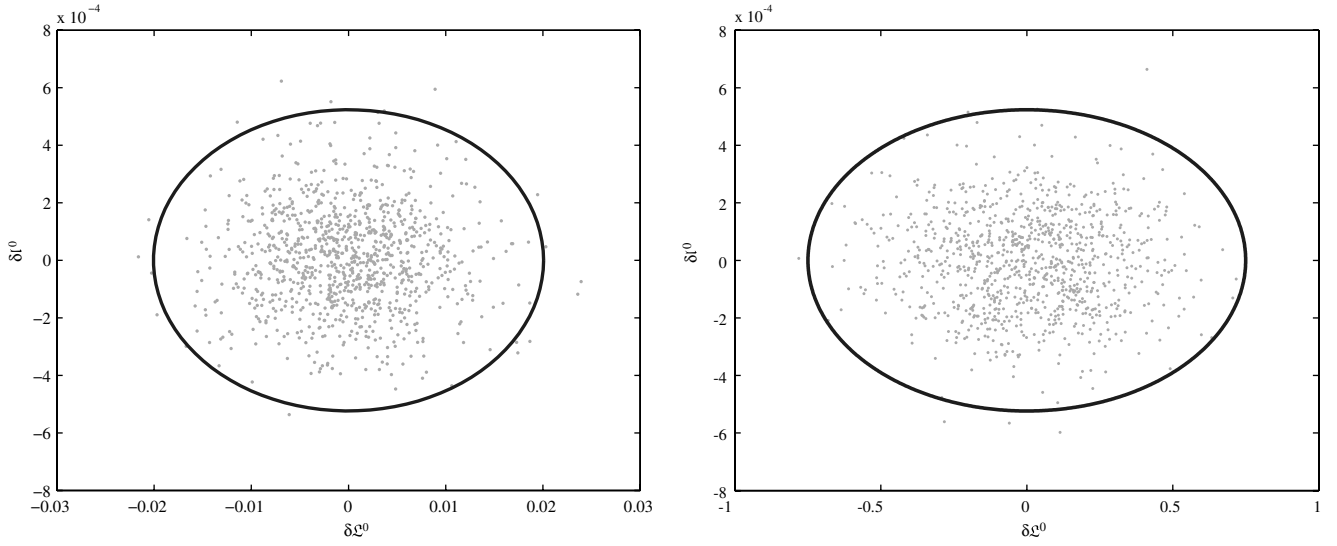

Fig. 1 Initial Gaussian distribution in the $\delta\mathfrak{L}^0$-$\delta\mathfrak{l}^0$ plane (sampled with the gray points) with the corresponding 3-σ ellipse (dark curve) for cases 1 (left) and 2 (right).

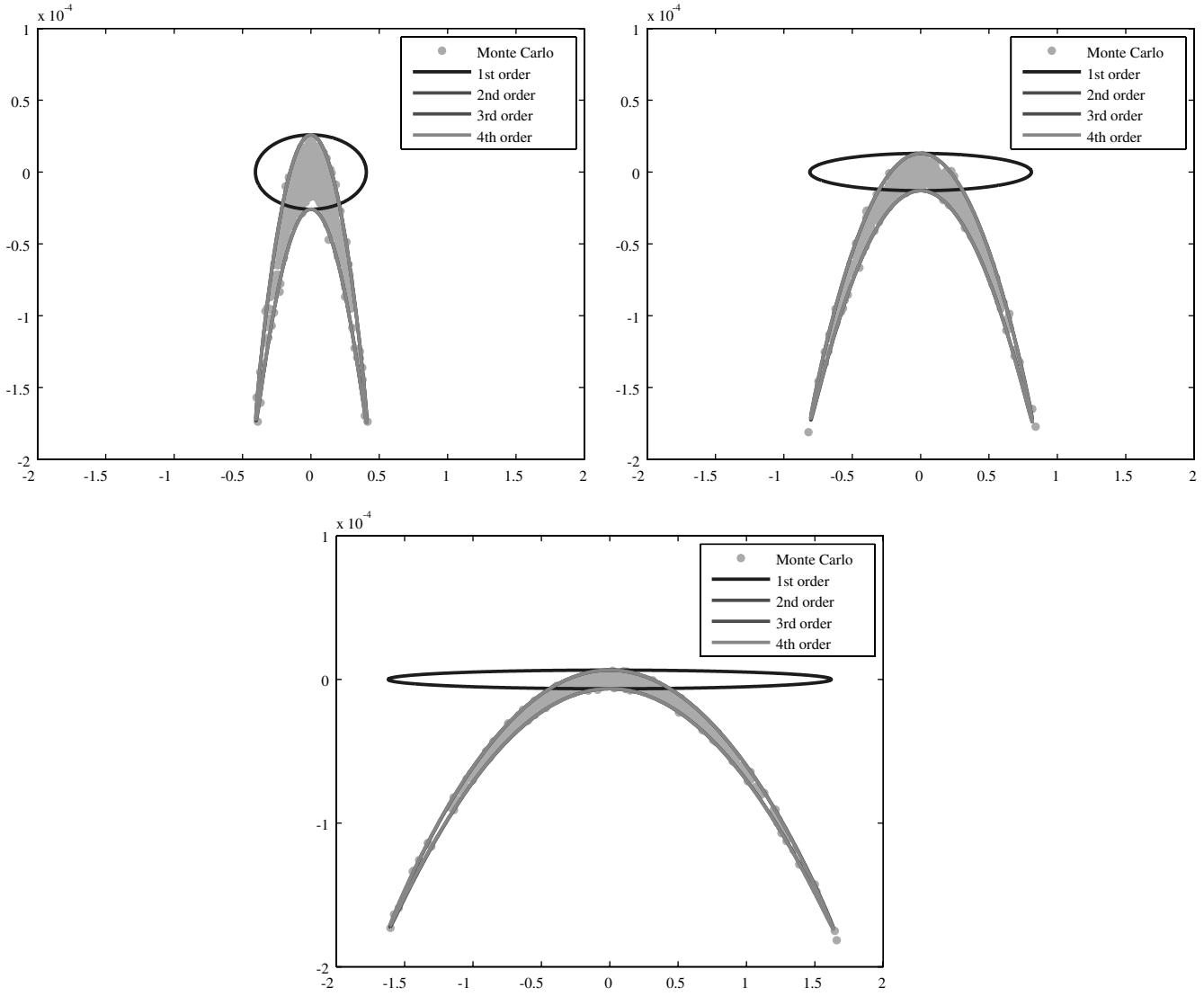

Fig. 2 The Gaussian distribution propagated for five (top left), 10 (top right), and 20 (bottom) orbit periods using various propagation methods for case 1. The $\delta\Omega$-δi plane is rotated so that the axes of the plot correspond to the principal axis directions of the linearly propagated ellipse. The second-order and higher curves are nearly identical. Points from the Monte Carlo run (labeled "Monte Carlo") represent the complete nonlinear dynamics. The lines (labeled "*n* order") represent how the edges of the initial 3-σ ellipse propagate with *n*-th-order STTs.

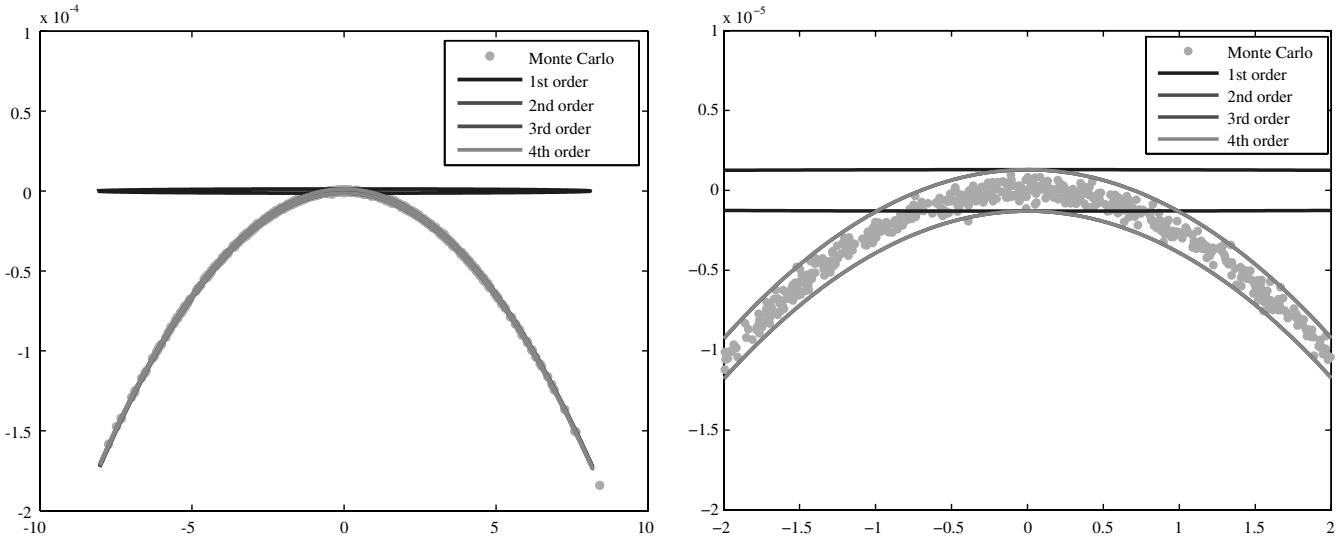

Fig. 3 The Gaussian distribution propagated for 100 orbital periods using various propagation methods. The figure on the right is a zoom up near the origin.

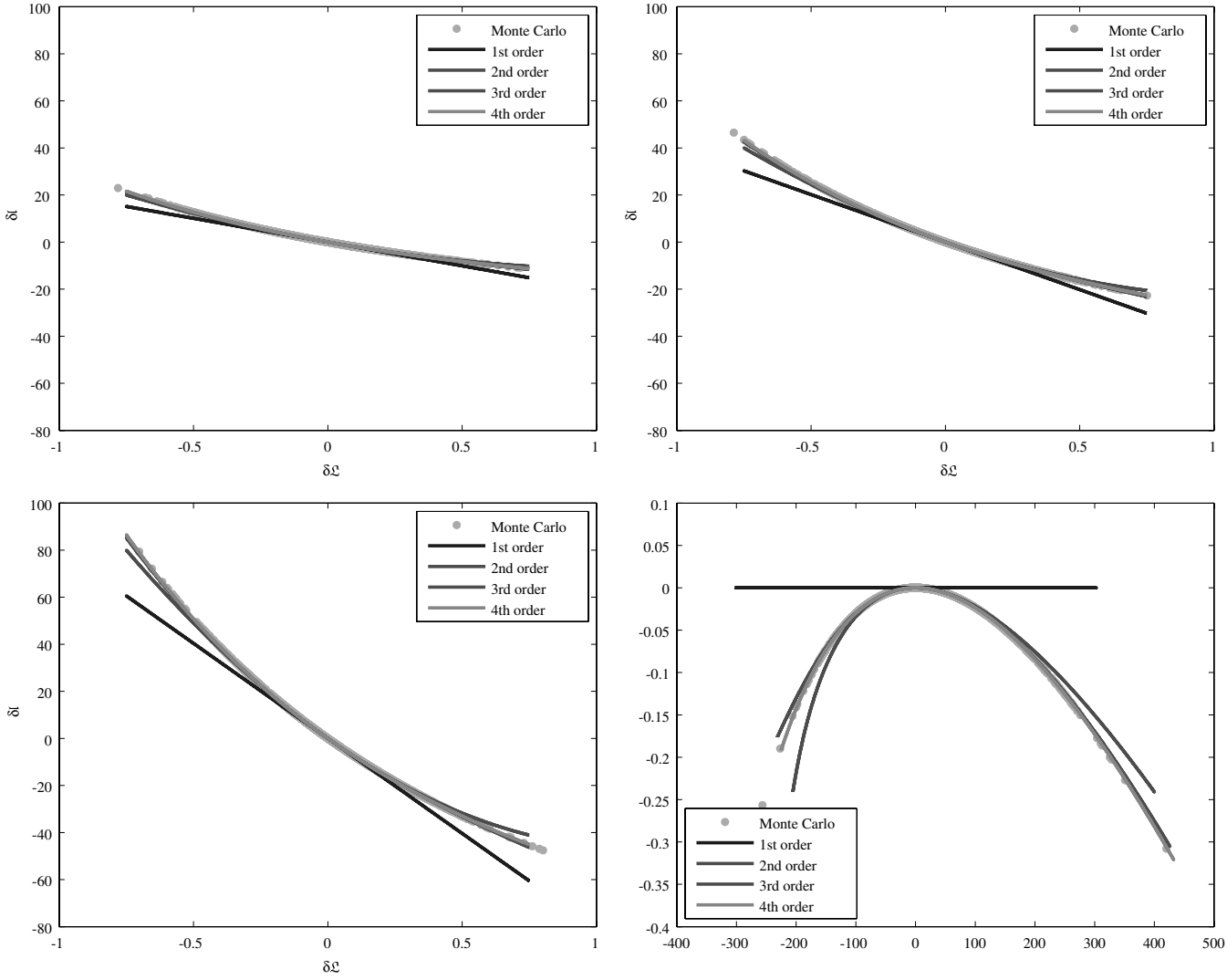

Fig. 4 The Gaussian distribution propagated for five (top left), 10 (top right), 20 (bottom left), and 100 orbit periods (bottom right) using various propagation methods for case 2. The second-order and higher curves are nearly identical. The figure for 100 orbit periods has been rotated as in Fig. 2.

$$[P] = \text{diag}(\sigma_a^2, \sigma_e^2, \sigma_i^2, \sigma_\Omega^2, \sigma_\omega^2, \sigma_M^2) \tag{45}$$

$$= \text{diag}(9.8328 \times 10^{-6}, 2.5 \times 10^{-5}, 3.0462 \times 10^{-6}, 3.0462 \times 10^{-6}, 3.0462 \times 10^{-6}, 3.0462 \times 10^{-8}) \tag{46}$$

where diag represents a diagonal matrix with the entries on the diagonal. This value corresponds to a 1-σ uncertainty of 20 km in a; 0.005 in e; 0.1 ° in i, Ω, and ω; and 0.01 ° in M. Figure 5 is a representation of this initial distribution in Poincaré space.

Figure 6 shows the results of the propagation. To highlight the effects on the uncertainties due to only the averaged J_2 term, the point-mass gravity term is omitted from the dynamics. For the Monte Carlo simulation, 10^4 points are distributed to be consistent with the initial uncertainty are generated and propagated using the complete averaged J_2 dynamics. For the STT propagation, 3.2×10^6 points are taken on the initial 3-σ hyper-ellipsoid and propagated using the approximate averaged J_2 dynamics up to first-order. The dynamics due to the J_2 gravity field harmonics are slow enough so that, even after 20 orbit periods ($\sim$32 hrs), a linear propagation of the uncertainty is consistent. Therefore, oftentimes for the problem of two-body dynamics+averaged J_2 perturbations, it is necessary to include second-order and higher expansions of only the point-mass gravity term. This is indeed the case in Fig. 7; when the two-body dynamics are included via STTs up to second-order, the Monte Carlo points remain included in the propagated 3-σ hyper-ellipsoid.

B. Comparison of the Mean and Covariance Matrix

Here, results of the mean and covariance matrix propagated using STTs and those computed by a Monte Carlo sampling of the uncertainty are compared. Note that for the former, the results are strictly analytical in that no sampling was required; refer to Eq. (22) and (23). Only two-body dynamics are considered for this example. The truth trajectory is the same as Eq. (40), and an initial zero-mean Gaussian distribution is assumed. Solely due to limitations of the random number generator in MATLAB, only the covariance matrix for case 2, or Eq. (42), is considered. For the Monte Carlo results, the mean and covariance matrices from 100 Monte Carlo runs are averaged, with each run consisting of 10^6 sample points. Table 1 compares the propagated mean after 5, 10, 20, and 100 orbits, and Table 2, the covariance matrix.

The mean changes only in the $\mathfrak{l}$-direction for Monte Carlo and high-order STT propagation, which is expected, as two-body dynamics influences only the mean longitude. Similarly, the covariance matrix changes only for the variance of $\mathfrak{l}$ and the covariance between $\mathfrak{L}$ and $\mathfrak{l}$. The error in the mean and covariance matrix becomes smaller as the order of propagation increases, as expected, but two interesting points are noted. First, the value of the mean is equal when using either second-order or third-order dynamics. This is because, from Eq. (22), the difference between the two orders are the terms involving the initial third-order moment of the PDF. Now, if assuming an initial Gaussian distribution, Eq. (27) for the third-order moment, as presented by Park and Scheeres [4], is

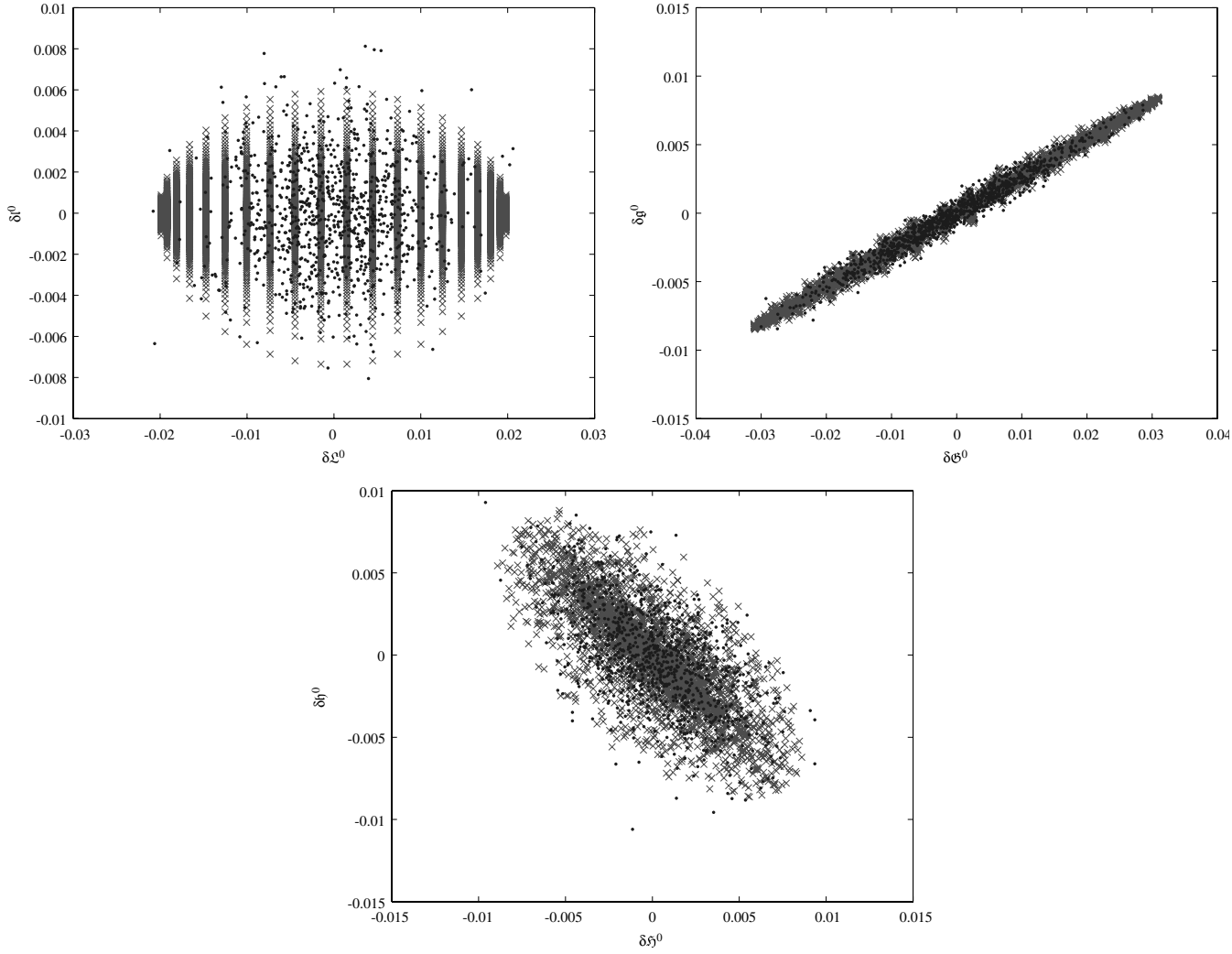

Fig. 5 Initial Gaussian distribution (sampled with the darker points) projected onto the $\delta\Omega^0$-δI^0 (top left), δG^0-δg^0 (top right), and $\delta\Theta^0$-δh^0 (bottom) subspaces with the corresponding 3-σ hyper-ellipsoid (sampled with lighter points).

$$\kappa^{i_1 i_2 i_3} = \kappa^{i_1}\kappa^{i_2}\kappa^{i_3} + (\kappa^{i_1}\kappa^{i_2,i_3} + \kappa^{i_2}\kappa^{i_1 i_3} + \kappa^{i_3}\kappa^{i_1,i_2}) \tag{47}$$

But zero initial mean (i.e., first-order cumulant) was also assumed, so $\kappa^{i_1 i_2 i_3} = 0$, and the third-order does not contribute to the polynomial expansion. In fact, any odd-order expansion of the dynamics greater than or equal to order 3 will result in the same propagated mean as the even-order expansion of one less order.

Second, the relative error of the mean, variance, and covariance remain almost constant as the propagation time is increased. This does not imply, however, that the PDF remains consistent for all time even for low-order STTs, as is demonstrated in section IV.A. Consider first the mean. From Eq. (14) and (31), the state deviation, $\delta\tilde{\mathfrak{I}}$, in the $\mathfrak{I}$-direction at time, t, found from STTs can be written as

$$\delta\tilde{\mathfrak{I}}(t) = (\Phi_{\mathfrak{I},\Omega}\delta\Omega^0 + \Phi_{\mathfrak{I},\mathfrak{I}}\delta\mathfrak{I}^0) + \frac{1}{2}\Phi_{\mathfrak{I},\Omega\Omega}(\delta\Omega^0)^2 + \ldots \tag{48}$$

$$= \delta\mathfrak{I}^0 - 3(\Omega^0)^{-4}\mu^2\Delta t(\delta\Omega^0) + 6(\Omega^0)^{-5}\mu^2\Delta t(\delta\Omega^0)^2 + \ldots \tag{49}$$

where $\delta\Omega^0$ and $\delta\mathfrak{I}^0$ are the initial state deviations. Factoring out all of the terms with Δt,

$$\delta\tilde{\mathfrak{I}}(t) = \delta\mathfrak{I}^0 + \delta\hat{\mathfrak{I}}\Delta t \tag{50}$$

$\delta\hat{\mathfrak{I}}$ is constant in time. Next, from the complete two-body dynamics, the deviation $\delta\mathfrak{I}$ is

$$\delta\mathfrak{I}(t) = \delta\mathfrak{I}^0 + \mu^2\{(\Omega^0)^{-3} - (\Omega^0_*)^{-3}\}\Delta t \tag{51}$$

where the asterisk denotes the reference orbit. Therefore, the absolute error between the mean calculated using Monte Carlo runs and using STTs is

$$\begin{aligned} E[\delta\mathfrak{I}(t)] - E[\delta\tilde{\mathfrak{I}}(t)] &= E[\delta\mathfrak{I}(t) - \delta\tilde{\mathfrak{I}}(t)] \\ &= E[\mu^2\{(\Omega^0)^{-3} - (\Omega^0_*)^{-3}\} - \delta\hat{\mathfrak{I}}]\Delta t \end{aligned} \tag{52}$$

which grows proportionally with propagation time. The relative error is then

$$\frac{E[\delta\mathfrak{I}(t)] - E[\delta\tilde{\mathfrak{I}}(t)]}{E[\delta\mathfrak{I}(t)]} = \frac{E[\mu^2\{(\Omega^0)^{-3} - (\Omega^0_*)^{-3}\} - \delta\hat{\mathfrak{I}}]\Delta t}{E[\delta\mathfrak{I}^0 + \mu^2\{(\Omega^0)^{-3} - (\Omega^0_*)^{-3}\}\Delta t]} \tag{53}$$

But, initially zero-mean, so $E[\delta\mathfrak{I}^0] = 0$, and denoting $S \equiv \mu^2\{(\Omega^0)^{-3} - (\Omega^0_*)^{-3}\}$ constant in time,

$$\frac{E[\delta\mathfrak{I}(t)] - E[\delta\tilde{\mathfrak{I}}(t)]}{E[\delta\mathfrak{I}(t)]} = \frac{(E[S] - E[\delta\hat{\mathfrak{I}}])\Delta t}{E[\delta\mathfrak{I}^0] + E[S]\Delta t} = 1 - \frac{E[\delta\hat{\mathfrak{I}}]}{E[S]} \tag{54}$$

which does not depend on propagation time, as the results indicate. $E[\delta\hat{\mathfrak{I}}]$ and $E[S]$ can both be determined a priori; thus, it is possible to estimate the amount of relative error the mean of a PDF will incur at an arbitrary order of the dynamics simply given the initial reference state and information regarding the initial probability distribution.

Next, for the variance $\sigma^2_{\mathfrak{I}}$,

$$\sigma^2_{\mathfrak{I}} = E[(\delta\mathfrak{I} - \bar{\delta\mathfrak{I}})^2] = E[\delta\mathfrak{I}^2] - \bar{\delta\mathfrak{I}}^2 \tag{55}$$

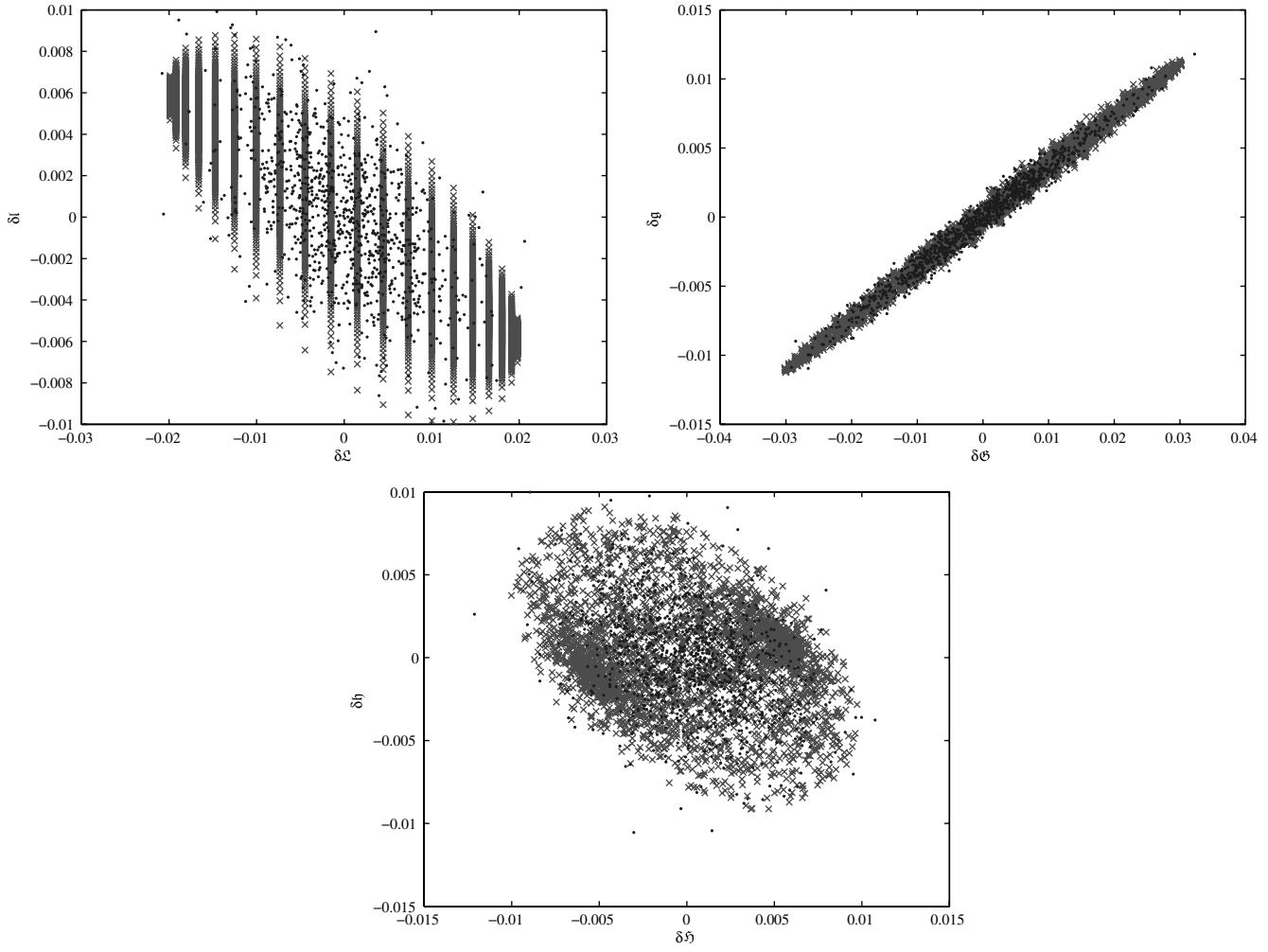

Fig. 6 The Gaussian distribution propagated for 20 orbital periods and projected onto the $\delta\mathfrak{L}$-$\delta\mathfrak{l}$ (top left), $\delta\mathfrak{G}$-$\delta\mathfrak{g}$ (top right), and $\delta\mathfrak{H}$-$\delta\mathfrak{h}$ (bottom) subspaces. Monte Carlo results in darker points, and STT propagation results in lighter points.

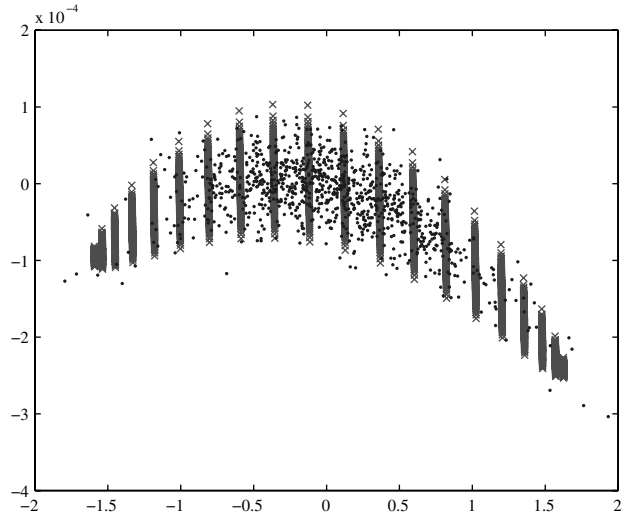

Fig. 7 The Gaussian distribution propagated for 20 orbital periods using a second-order expansion of the two-body dynamics+a first-order expansion of the averaged perturbation due to J_2. The distribution is projected onto the $\delta\mathfrak{L}$-$\delta\mathfrak{l}$ subspace, then rotated so that the axes of the plot correspond to the principal axis directions of the propagated covariance matrix. Monte Carlo results in darker points, and STT propagation results in lighter points.

where the bar indicates mean. Now, for the complete two-body dynamics,

$$E[\delta\mathfrak{l}^2] = (\delta\mathfrak{l}^0)^2 - \frac{2\delta\mathfrak{l}^0\mu^2}{(\mathfrak{L}^0_*)^3}\Delta t + \frac{\mu^4}{(\mathfrak{L}^0_*)^6}\Delta t^2 + 2\delta\mathfrak{l}^0\mu^2 E[(\mathfrak{L}^0)^{-3}]\Delta t - \frac{2\mu^4}{(\mathfrak{L}^0_*)^3}E[(\mathfrak{L}^0)^{-3}]\Delta t^2 + \mu^4 E[(\mathfrak{L}^0)^{-6}]\Delta t^2 \tag{56}$$

$$\delta\tilde{\mathfrak{l}}^2 = (\delta\mathfrak{l}^0)^2 - \frac{2\delta\mathfrak{l}^0\mu^2}{(\mathfrak{L}^0_*)^3}\Delta t + \frac{\mu^4}{(\mathfrak{L}^0_*)^6}\Delta t^2 + 2\delta\mathfrak{l}^0\mu^2 E[(\mathfrak{L}^0)^{-3}]\Delta t - \frac{2\mu^4}{(\mathfrak{L}^0_*)^3}E[(\mathfrak{L}^0)^{-3}]\Delta t^2 + \mu^4 (E[(\mathfrak{L}^0)^{-3}])^2\Delta t^2 \tag{57}$$

Therefore,

$$\sigma^2_{\mathfrak{l}} = \mu^4\{E[(\mathfrak{L}^0)^{-6}] - (E[(\mathfrak{L}^0)^{-3}])\}\Delta t^2 \equiv \mu^4 E[K]\Delta t^2 \tag{58}$$

Next, for the approximate dynamics from the STTs,

$$E[\delta\tilde{\mathfrak{l}}^2] = (\delta\mathfrak{l}^0)^2 + 2\delta\mathfrak{l}^0 E[\delta\hat{\mathfrak{l}}]\Delta t + E[\delta\hat{\mathfrak{l}}^2]\Delta t^2 \tag{59}$$

$$(E[\delta\tilde{\mathfrak{l}}])^2 = (\delta\mathfrak{l}^0)^2 + 2\delta\mathfrak{l}^0 E[\delta\hat{\mathfrak{l}}]\Delta t + (E[\delta\hat{\mathfrak{l}}])^2\Delta t^2 \tag{60}$$

Thus,

$$\tilde{\sigma}^2_{\mathfrak{l}} = \{E[\delta\hat{\mathfrak{l}}^2] - (E[\delta\hat{\mathfrak{l}}])^2\}\Delta t^2 \equiv E[\hat{K}]\Delta t^2 \tag{61}$$

The relative error is

Table 1 The mean $\delta\bar{\mathfrak{l}}$ of the deviation of Poincaré element, $\mathfrak{l}$, for different numerical and analytical propagation methods. "Δ [%]" indicates relative error with respect to the Monte Carlo results in percentages

	Monte Carlo	First order		Second order		Third order		Fourth order	
	$\delta\bar{\mathfrak{l}}$	$\delta\bar{\mathfrak{l}}$	Δ [%]	$\delta\bar{\mathfrak{l}}$	Δ [%]	$\delta\bar{\mathfrak{l}}$	Δ [%]	$\delta\bar{\mathfrak{l}}$	Δ [%]
5 orbits	0.5521	0	100	0.5401	2.176	0.5401	2.176	0.5517	0.074
10 orbits	1.1042	0	100	1.0802	2.176	1.0802	2.176	1.1034	0.074
20 orbits	2.2084	0	100	2.1604	2.176	2.1604	2.176	2.2068	0.074
100 orbits	11.042	0	100	10.802	2.176	10.802	2.176	11.034	0.074

Table 2 Elements from the covariance matrix for different numerical and analytical propagation methods

	Monte Carlo		First order				Third order			
	$\mu_{\mathfrak{l}\mathfrak{L}}$	$\sigma_{\mathfrak{l}}^2$	$\mu_{\mathfrak{l}\mathfrak{L}}$	Δ [%]	$\sigma_{\mathfrak{l}}^2$	Δ [%]	$\mu_{\mathfrak{l}\mathfrak{L}}$	Δ [%]	$\sigma_{\mathfrak{l}}^2$	Δ [%]
5 orbits	−1.2975	27.626	−1.2605	2.851	25.451	7.871	−1.2966	0.068	27.528	0.353
10 orbits	−2.5951	110.50	−2.5211	2.851	101.80	7.871	−2.5933	0.068	110.11	0.353
20 orbits	−5.1902	442.01	−5.0422	2.851	407.22	7.871	−5.1867	0.068	440.45	0.353
100 orbits	−25.951	11050	−25.211	2.851	10181	7.871	−25.933	0.068	11011	0.353

$$\frac{\sigma_{\mathfrak{l}}^2 - \tilde{\sigma}_{\mathfrak{l}}^2}{\sigma_{\mathfrak{l}}^2} = 1 - \frac{E[\hat{K}]}{\mu^4 E[K]} \tag{62}$$

which, again, is independent of the propagation time.

Finally, for the covariance, $\mu_{\mathfrak{l}\mathfrak{L}}$,

$$\mu_{\mathfrak{l}\mathfrak{L}} = E[(\delta\mathfrak{l} - \delta\bar{\mathfrak{l}})(\delta\mathfrak{L} - \delta\bar{\mathfrak{L}})] = E[\delta\mathfrak{l}\delta\mathfrak{L}] - \delta\bar{\mathfrak{l}}\delta\bar{\mathfrak{L}} \tag{63}$$

$$\tilde{\mu}_{\mathfrak{l}\mathfrak{L}} = E[(\delta\tilde{\mathfrak{l}} - E[\delta\tilde{\mathfrak{l}}])(\delta\mathfrak{L} - \delta\bar{\mathfrak{L}})] = E[\delta\tilde{\mathfrak{l}}\delta\mathfrak{L}] - E[\delta\tilde{\mathfrak{l}}]\delta\bar{\mathfrak{L}} \tag{64}$$

But $\delta\mathfrak{L} = \delta\mathfrak{L}^0$, so $E[\delta\mathfrak{l}\delta\mathfrak{L}] = E[\delta\mathfrak{l}\delta\mathfrak{L}^0]$, and $\delta\bar{\mathfrak{L}} = \delta\bar{\mathfrak{L}}^0 = 0$ from the zero initial mean assumption. Next, from Eq. (50) and (51),

$$E[\delta\mathfrak{l}\delta\mathfrak{L}^0] = E[\delta\mathfrak{L}^0(\delta\mathfrak{l}^0 + S\Delta t)] = E[\delta\mathfrak{L}^0\delta\mathfrak{l}^0] + E[\delta\mathfrak{L}^0 S]\Delta t \tag{65}$$

$$E[\delta\tilde{\mathfrak{l}}\delta\mathfrak{L}^0] = E[\delta\mathfrak{L}^0(\delta\mathfrak{l}^0 + \delta\hat{\mathfrak{l}}\Delta t)] = E[\delta\mathfrak{L}^0\delta\mathfrak{l}^0] + E[\delta\mathfrak{L}^0\delta\hat{\mathfrak{l}}]\Delta t \tag{66}$$

where both $E[\delta\mathfrak{L}^0\delta\hat{\mathfrak{l}}]$ and $E[\delta\mathfrak{L}^0 S]$ are constants in time. In addition, recall that for this particular example, the initial covariance is 0 (i.e., off-diagonals of the covariance matrix is 0), so $E[\delta\mathfrak{L}^0\delta\mathfrak{l}^0] = 0$. As a consequence, the relative error is

$$\frac{\mu_{\mathfrak{l}\mathfrak{L}} - \tilde{\mu}_{\mathfrak{l}\mathfrak{L}}}{\mu_{\mathfrak{l}\mathfrak{L}}} = 1 - \frac{E[\delta\mathfrak{L}^0\delta\hat{\mathfrak{l}}]}{E[\delta\mathfrak{L}^0 S]} \tag{67}$$

which is independent of the propagation time.

C. Conservation of the Prediction Error

Here, a comparison is conducted of how well the uncertainty consistency metric Eq. (13) is conserved when 1) the proposed approach of propagating the PDFs with the solution to the Fokker-Planck Eq. (8) for deterministic Hamiltonian systems is implemented, and 2) the classical approach of propagating only the first two cumulants linearly along a reference trajectory with the state transition matrix Eq. (12) is implemented. Recall from section II.A that the more $\mathcal{PE}(t)$ changes with propagation time, the less accurate the representation of the uncertainty becomes. Of the two truth orbits to be considered, the initial state of the first (object 1) is Eq. (40), and the second (object 2) is given as

$$a = 1.10064, \qquad e = i = \Omega = \omega = M = 0 \Rightarrow \mathfrak{L} = 4.6812$$
$$\mathfrak{l} = \mathfrak{G} = \mathfrak{g} = \mathfrak{H} = \mathfrak{h} = 0 \tag{68}$$

The same two initial Gaussian distributions as in section IV.A are assumed for the uncertainty of both orbits to define PDFs, $p_1(\mathbf{X}^0)$ and $p_2(\mathbf{X}^0)$, as zero-mean and covariance matrices given in Eq. (41) and (42) (cases 1 and 2, respectively). Only two-body dynamics are considered for this example.

To compute $\mathcal{PE}(t)$: 1) Fokker-Planck:

a) Propagate initial PDFs with forward flow, $\boldsymbol{\phi}(t; \mathbf{X}^0, t^0)$;

b) Sample PDFs and propagate each point back to time, t^0, with either the complete inverse flow, $\boldsymbol{\psi}(t, \mathbf{X}; t^0)$, or its corresponding STT, Ψ;

c) Evaluate the PDF at each $\mathbf{X}^0$ and assign this value to $\mathbf{X}$; and

d) Numerically integrate $p_1 p_2$ over state space $\mathbf{X}$.

2) Linear:

a) Propagate the mean and covariance matrices of the initial PDFs with the STM;

b) Sample PDFs and evaluate it at each sample point; and

c) Numerically integrate $p_1 p_2$ over state space $\mathbf{X}$.

Figure 8 shows the evolution of $\mathcal{PE}(t)$ over 20 orbit periods of object 1 for both methods, and Table 3 is a summary of $\mathcal{PE}(t)$ after 20 orbit periods. As expected, $\mathcal{PE}(t)$ is best conserved for method 1 with complete inverse dynamics, followed by that with the higher-order STT dynamics. Also, for case 1, the solution from method 1 with first-order STTs and those from method 2 are nearly equivalent, and their uncertainty consistency is considerably worse than all of the other methods. With the increased uncertainty in case 2, the results from method 1 with first-order STTs and method 2, although no longer equivalent after 20 orbits, both begin to diverge from the initial value in a concave-down sense after about five orbits. On the other hand, this behavior is not observed for PDFs propagated using method 2 with second-order dynamics and higher. These results quantify the robustness of the proposed method of uncertainty propagation that was mentioned in section IV.A.

Again, linear propagation of uncertainty becomes inconsistent with the actual probability distribution even after a couple of orbits. Furthermore, the performance improvement diminishes for propagation via the Fokker-Planck solution as the order of the inverse STT dynamics is increased. These results suggest that second-order dynamics may provide sufficient uncertainty

Table 3 Change in $\mathcal{PE}$ after 20 orbit periods of object 1 for case 1. "F-P" indicates propagation via the Fokker-Planck solution, and the number after "STT" indicates the order of the expansion of the dynamics

	Linear	F-P (STT:1)	F-P (STT:2)	F-P (STT:3)	F-P (STT:4)	F-P (Complete)
$\Delta\mathcal{PE}$	23725.31	23725.31	116.8219	0.003063	8.71507×10^{-5}	3.82374×10^{-6}

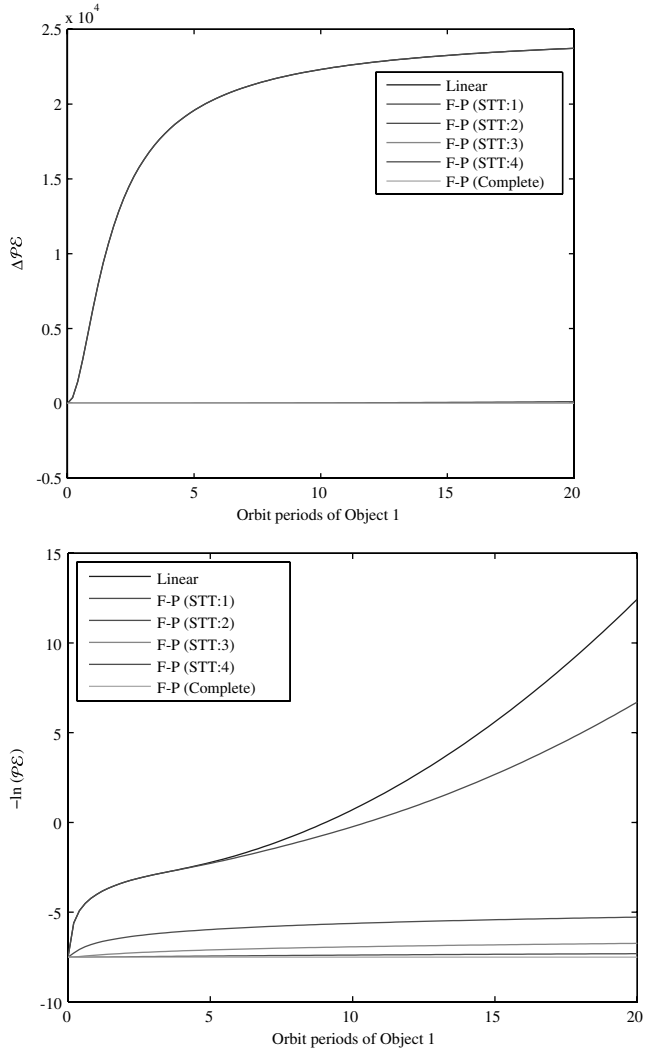

Fig. 8 The change in $\mathcal{PE}(t)$ over time using various propagation methods for case 1 (top) and case 2 (bottom). For case 1, the linear and F-P (STT:1) curves and the F-P (STT:2) through F-P (Complete) curves are nearly identical, respectively. For case 2, a log scale is used due to the larger spread of values compare to case 1.

consistency for many applications. For the two-body problem, the C ++ implementation is able to generate both first- and second-order STTs in less than a second on a Core 2 Duo laptop. Even for more complex dynamical systems that do not have analytical solution flows, only $6^2 + 6^3 = 252$ ordinary differential equations in Eq. (17) need to be solved to generate STTs up to second-order. The proposed method has the potential of consistently propagating PDFs with less computational burden than existing techniques. For example, an Edgeworth filter attaining the same level of accuracy as the second-order STT requires the evaluation of 2021 sigma points [2]. Furthermore, unlike a Monte Carlo analysis, where the dynamics must be integrated for every sample point of every epoch, the STT needs to be integrated only once per epoch [4,7].

V. Conclusion

In this paper, recent developments in analytical nonlinear propagation of uncertainty for deterministic Hamiltonian dynamical systems were applied to the two-body problem. For such systems, as a consequence of the solution of the Fokker-Planck equation, the probability density function can be analytically propagated as long as an analytical expression for the initial probability density function and the solution flow of the dynamics exist. One way of obtaining an analytical dynamics solution is to use the STT concept, which is a Taylor series expansion of the dynamics to arbitrary order. Numerical results show that this method is, with reasonable computational burden, capable of propagating uncertainty while maintaining consistency. Potential applications include more robust correlation of optical tracks and initial orbit determination via the admissible region concept.

Future work is needed to develop ways to incorporate more complex dynamical models, such as the full perturbation due to a nonspherical gravity field, or effects due to nonconservative forces.

Appendix A: State Transition Matrix for Averaged J_2 Perturbation

Let $\Phi_P = (\partial^P \mathbf{X}(t)/\partial^P \mathbf{X}^0)$, $\Phi_D = (\partial^D \mathbf{X}(t)/\partial^D \mathbf{X}^0)$, $J_{PD} = \{\partial^P \mathbf{X}(t)/\partial^D \mathbf{X}(t)\}$, and $J_{DP,0} = (\partial^D \mathbf{X}^0/\partial^P \mathbf{X}^0)$. Then,

$$\Phi_P = J_{PD} \circ \Phi_D \circ J_{DP,0} \tag{A1}$$

Φ_D has no singularities

$$\Phi_D(1,1) = \Phi_D(2,2) = \Phi_D(3,3) = \Phi_D(4,4) = \Phi_D(5,5) = \Phi_D(6,6) = 1 \tag{A2}$$

$$\Phi_D(2,1) = \left[-\frac{3\mu^2}{L^4} + J_2\left(\frac{3\mu^4 r_E^2}{L^8}\right)\left(\frac{L}{G}\right)^3\left(1 - 3\frac{H^2}{G^2}\right)\right]t \tag{A3}$$

$$\Phi_D(2,3) = \Phi_D(4,1) = J_2\left(\frac{9\mu^4 r_E^2}{4L^8}\right)\left(\frac{L}{G}\right)^4\left(1 - 5\frac{H^2}{G^2}\right)t \tag{A4}$$

$$\Phi_D(2,5) = J_2\left(\frac{9\mu^4 r_E^2}{2L^8}\right)\left(\frac{L}{G}\right)^4\left(\frac{H}{G}\right)t \tag{A5}$$

$$\Phi_D(4,3) = J_2\left(\frac{3\mu^4 r_E^2}{2L^8}\right)\left(\frac{L}{G}\right)^5\left(2 - 15\frac{H^2}{G^2}\right)t \tag{A6}$$

$$\Phi_D(4,5) = \Phi_D(6,3) = J_2\left(\frac{15\mu^4 r_E^2}{2L^8}\right)\left(\frac{L}{G}\right)^5\left(\frac{H}{G}\right)t \tag{A7}$$

$$\Phi_D(6,1) = J_2\left(\frac{9\mu^4 r_E^2}{2L^8}\right)\left(\frac{L}{G}\right)^4\left(\frac{H}{G}\right)t \tag{A8}$$

$$\Phi_D(6,5) = -J_2\left(\frac{3\mu^4 r_E^2}{2L^8}\right)\left(\frac{L}{G}\right)^4 t \tag{A9}$$

Unless otherwise stated, only nonzero elements of a matrix are listed in this section. J_{PD} and $J_{DP,0}$, on the other hand, can contain $0/0$ singularities

$$J_{PD}(1,1) = J_{PD}(2,2) = J_{PD}(2,4) = J_{PD}(2,6) = 1$$
$$J_{DP,0}(1,1) = J_{DP,0}(2,2) = J_{DP,0}(3,1) = J_{DP,0}(5,1) = 1 \tag{A10}$$

$$J_{PD}(4,4) = J_{PD}(4,6) = \mathfrak{G} \qquad J_{DP,0}(3,3) = J_{DP,0}(5,3) = -\mathfrak{G}^0 \tag{A11}$$

$$J_{PD}(3,4) = -J_{PD}(3,6) = -\mathfrak{g} \qquad J_{DP,0}(3,4) = J_{DP,0}(5,4) = -\mathfrak{g}^0 \tag{A12}$$

$$J_{PD}(6,6) = \mathfrak{H} \qquad J_{DP,0}(5,5) = -\mathfrak{H}^0 \tag{A13}$$

$$J_{PD}(5,6) = -\mathfrak{h} \qquad J_{DP,0}(5,6) = -\mathfrak{h}^0 \tag{A14}$$

$$J_{PD}(3,1) = -J_{PD}(3,3) = \frac{\mathfrak{G}}{\mathfrak{G}^2 + \mathfrak{g}^2}$$

$$J_{DP,0}(2,4) = J_{DP,0}(4,4) = -\frac{\mathfrak{G}^0}{(\mathfrak{G}^0)^2 + (\mathfrak{g}^0)^2} \tag{A15}$$

$$J_{PD}(4,1) = -J_{PD}(4,3) = \frac{\mathfrak{g}}{\mathfrak{G}^2 + \mathfrak{g}^2}$$

$$J_{DP,0}(2,3) = -J_{DP,0}(4,3) = \frac{\mathfrak{g}^0}{(\mathfrak{G}^0)^2 + (\mathfrak{g}^0)^2} \tag{A16}$$

$$J_{PD}(5,3) = -J_{PD}(5,5) = \frac{\mathfrak{H}}{\mathfrak{H}^2 + \mathfrak{h}^2}$$

$$J_{DP,0}(4,6) = -J_{DP,0}(6,6) = -\frac{\mathfrak{H}^0}{(\mathfrak{H}^0)^2 + (\mathfrak{h}^0)^2} \tag{A17}$$

$$J_{PD}(6,3) = -J_{PD}(6,5) = \frac{\mathfrak{h}}{\mathfrak{H}^2 + \mathfrak{h}^2}$$

$$J_{DP,0}(5,4) = -J_{DP,0}(6,5) = \frac{\mathfrak{h}^0}{(\mathfrak{H}^0)^2 + (\mathfrak{h}^0)^2} \tag{A18}$$

But these singularities cancel out when Φ_P is computed

$$\Phi_P(1,1) = 1 \tag{A19}$$

$$\Phi_P(2,1) = \Phi_D(2,1) + \Phi_D(2,3) + \Phi_D(2,5) + \Phi_D(4,1) + \Phi_D(4,3) + \Phi_D(4,5) + \Phi_D(6,1) + \Phi_D(6,3) + \Phi_D(6,5) \tag{A20}$$

$$\Phi_P(2,3) = -\mathfrak{G}^0\{\Phi_D(2,3) + \Phi_D(4,3) + \Phi_D(6,3) + \Phi_D(2,5) + \Phi_D(4,5) + \Phi_D(6,5)\} \tag{A21}$$

$$\Phi_P(2,4) = -\mathfrak{g}^0\{\Phi_D(2,3) + \Phi_D(4,3) + \Phi_D(6,3) + \Phi_D(2,5) + \Phi_D(4,5) + \Phi_D(6,5)\} \tag{A22}$$

$$\Phi_P(2,5) = -\mathfrak{H}^0\{\Phi_D(2,5) + \Phi_D(4,5) + \Phi_D(6,5)\} \tag{A23}$$

$$\Phi_P(2,6) = -\mathfrak{h}^0\{\Phi_D(2,5) + \Phi_D(4,5) + \Phi_D(6,5)\} \tag{A24}$$

$$\Phi_P(3,1) = -\mathfrak{g}\{\Phi_D(4,1) + \Phi_D(4,3) + \Phi_D(4,5) + \Phi_D(6,1) + \Phi_D(6,3) + \Phi_D(6,5)\} \tag{A25}$$

$$\Phi_P(3,3) = \frac{\mathfrak{G}\mathfrak{G}^0}{\mathfrak{G}^2 + \mathfrak{g}^2} + \frac{\mathfrak{g}\mathfrak{g}^0}{(\mathfrak{G}^0)^2 + (\mathfrak{g}^0)^2}\mathfrak{G}^0\mathfrak{g}\{\Phi_D(4,3) + \Phi_D(4,5) + \Phi_D(6,3) + \Phi_D(6,5)\} \tag{A26}$$

$$= \cos\{(g - g^0) + (h - h^0)\} + \mathfrak{G}^0\mathfrak{g}\{\Phi_D(4,3) + \Phi_D(4,5) + \Phi_D(6,3) + \Phi_D(6,5)\} \tag{A27}$$

$$\Phi_P(3,4) = \frac{\mathfrak{G}\mathfrak{g}^0}{\mathfrak{G}^2 + \mathfrak{g}^2} - \frac{\mathfrak{g}\mathfrak{G}^0}{(\mathfrak{G}^0)^2 + (\mathfrak{g}^0)^2} + \mathfrak{g}^0\mathfrak{g}\{\Phi_D(4,3) + \Phi_D(4,5) + \Phi_D(6,3) + \Phi_D(6,5)\} \tag{A28}$$

$$= \sin\{(g - g^0) + (h - h^0)\} + \mathfrak{g}^0\mathfrak{g}\{\Phi_D(4,3) + \Phi_D(4,5) + \Phi_D(6,3) + \Phi_D(6,5)\} \tag{A29}$$

$$\Phi_P(3,5) = \mathfrak{g}\mathfrak{H}^0\{\Phi_D(4,5) + \Phi_D(6,5)\} \tag{A30}$$

$$\Phi_P(3,6) = \mathfrak{g}\mathfrak{h}^0\{\Phi_D(4,5) + \Phi_D(6,5)\} \tag{A31}$$

$$\Phi_P(4,1) = \mathfrak{G}\{\Phi_D(4,1) + \Phi_D(4,3) + \Phi_D(4,5) + \Phi_D(6,1) + \Phi_D(6,3) + \Phi_D(6,5)\} \tag{A32}$$

$$\Phi_P(4,3) = \frac{\mathfrak{g}\mathfrak{G}^0}{\mathfrak{g}^2 + \mathfrak{G}^2} - \frac{\mathfrak{G}\mathfrak{g}^0}{(\mathfrak{G}^0)^2 + (\mathfrak{g}^0)^2} - \mathfrak{G}^0\mathfrak{G}\{\Phi_D(4,3) + \Phi_D(4,5) + \Phi_D(6,3) + \Phi_D(6,5)\} \tag{A33}$$

$$= \sin\{(g - g^0) + (h - h^0)\} - \mathfrak{G}^0\mathfrak{G}\{\Phi_D(4,3) + \Phi_D(4,5) + \Phi_D(6,3) + \Phi_D(6,5)\} \tag{A34}$$

$$\Phi_P(4,4) = \frac{\mathfrak{g}\mathfrak{g}^0}{\mathfrak{G}^2 + \mathfrak{g}^2} + \frac{\mathfrak{G}\mathfrak{G}^0}{(\mathfrak{G}^0)^2 + (\mathfrak{g}^0)^2} - \mathfrak{g}^0\mathfrak{G}\{\Phi_D(4,3) + \Phi_D(4,5) + \Phi_D(6,3) + \Phi_D(6,5)\} \tag{A35}$$

$$= \cos\{(g - g^0) + (h - h^0)\} - \mathfrak{g}^0\mathfrak{G}\{\Phi_D(4,3) + \Phi_D(4,5) + \Phi_D(6,3) + \Phi_D(6,5)\} \tag{A36}$$

$$\Phi_P(4,5) = -\mathfrak{G}\mathfrak{H}^0\{\Phi_D(4,5) + \Phi_D(6,5)\} \tag{A37}$$

$$\Phi_P(4,6) = -\mathfrak{G}\mathfrak{h}^0\{\Phi_D(4,5) + \Phi_D(6,5)\} \tag{A38}$$

$$\Phi_P(5,1) = -\mathfrak{h}\{\Phi_D(6,1) + \Phi_D(6,3) + \Phi_D(6,5)\} \tag{A39}$$

$$\Phi_P(5,3) = \mathfrak{h}\mathfrak{G}^0\{\Phi_D(6,3) + \Phi_D(6,5)\} \tag{A40}$$

$$\Phi_P(5,4) = \mathfrak{h}\mathfrak{g}^0\{\Phi_D(6,3) + \Phi_D(6,5)\} \tag{A41}$$

$$\Phi_P(5,5) = \frac{\mathfrak{H}\mathfrak{H}^0}{\mathfrak{H}^2 + \mathfrak{h}^2} + \frac{\mathfrak{h}\mathfrak{h}^0}{(\mathfrak{H}^0)^2 + (\mathfrak{h}^0)^2} + \mathfrak{h}\mathfrak{H}^0\Phi_D(6,5) \tag{A42}$$

$$= \cos(h - h^0) + \mathfrak{h}\mathfrak{H}^0\Phi_D(6,5) \tag{A43}$$

$$\Phi_P(5,6) = \frac{\mathfrak{H}\mathfrak{h}^0}{\mathfrak{H}^2 + \mathfrak{h}^2} - \frac{\mathfrak{h}\mathfrak{H}^0}{(\mathfrak{H}^0)^2 + (\mathfrak{h}^0)^2} + \mathfrak{h}\mathfrak{h}^0\Phi_D(6,5) \tag{A44}$$

$$= -\sin(h - h^0) + \mathfrak{h}\mathfrak{h}^0\Phi_D(6,5) \tag{A45}$$

$$\Phi_P(6,1) = \mathfrak{H}\{\Phi_D(6,1) + \Phi_D(6,3) + \Phi_D(6,5)\} \tag{A46}$$

$$\Phi_P(6,3) = -\mathfrak{H}\mathfrak{G}^0\{\Phi_D(6,3) + \Phi_D(6,5)\} \tag{A47}$$

$$\Phi_P(6,4) = -\mathfrak{H}\mathfrak{g}^0\{\Phi_D(6,3) + \Phi_D(6,5)\} \tag{A48}$$

$$\Phi_P(6,5) = \frac{\mathfrak{h}\mathfrak{H}^0}{\mathfrak{H}^2 + \mathfrak{h}^2} - \frac{\mathfrak{H}\mathfrak{h}^0}{(\mathfrak{H}^0)^2 + (\mathfrak{h}^0)^2} - \mathfrak{H}\mathfrak{H}^0\Phi_D(6,5) \tag{A49}$$

$$= \sin(h - h^0) - \mathfrak{H}\mathfrak{H}^0\Phi_D(6,5) \tag{A50}$$

$$\Phi_P(6,6) = \frac{\mathfrak{h}\mathfrak{h}^0}{\mathfrak{H}^2 + \mathfrak{h}^2} + \frac{\mathfrak{H}\mathfrak{H}^0}{(\mathfrak{H}^0)^2 + (\mathfrak{h}^0)^2} - \mathfrak{H}\mathfrak{h}^0\Phi_D(5,6) \tag{A51}$$

$$= \cos(h - h^0) - \mathfrak{H}\mathfrak{h}^0\Phi_D(5,6) \tag{A52}$$

Note that the Delaunay angles only appear as a difference between the initial and current values, meaning that, because the rate of change of the angles are well defined and constant for any orbit, the differences are also well defined.

References

[1] Horwood, J., Aragon, N. D., and Poore, A. B., "Estimation of Drag and its Uncertainty in Initial Orbit Determination Using Gauss-Hermite Quadrature," *Presented at the AAS Born Symposium*, AAS, Boulder, CO, 2010.

[2] Horwood, J., Aragon, N. D., and Poore, A. B., "Edgeworth Filters For Space Surveillance Tracking," *Presented at the 2010 Advanced Maui Optical and Space Surveillance Technologies Conference*, AMOS, Wailea-Maui, HI, 2010.

[3] Tapley, B. D., Schutz, B. E., and Born, G. H., *Statistical Orbit Determination*, Elsevier Academic Press, Burlington, MA, 2004, pp. 159–284.

[4] Park, R. S., and Scheeres, D. J., "Nonlinear Mapping of Gaussian Statistics: Theory and Applications to Spacecraft Trajectory Design," *Journal of Guidance, Control, and Dynamics*, Vol. 29, No. 6, 2006, pp. 1367–1375. doi:10.2514/1.20177

[5] Junkins, J., Akella, M., and Alfriend, K. T., "Non-Gaussian Error Propagation in Orbit Mechanics," *Journal of the Astronautical Sciences*, Vol. 44, No. 4, 1996, pp. 541–563.

[6] Junkins, J., and Singla, P., "How Nonlinear is it? A tutorial on Nonlinearity of Orbit and Attitude Dynamics," *Journal of the Astronautical Sciences*, Vol. 52, No. 1, 2, 2004, pp. 7–60.

[7] Maybeck, P. S., *Stochastic Models, Estimation and Control*, Vol. 2, Academic Press, New York, NY, 1982, pp. 159–271.

[8] Maruskin, J. M., Scheeres, D. J., and Alfriend, K. T., "Correlation of Optical Observations of Objects in Earth Orbit," *Journal of Guidance, Control, and Dynamics*, Vol. 32, No. 1, 2009, pp. 194–209. doi:10.2514/1.36398

[9] Fujimoto, K., Maruskin, J. M., and Scheeres, D. J., "Circular and Zero-Inclination Solutions for Optical Observations of Earth-Orbiting Objects," *Celestial Mechanics and Dynamical Astronomy*, Vol. 106, No. 2, 2010, pp. 157–182. doi:10.1007/s10569-009-9245-y

[10] Fujimoto, K., and Scheeres, D. J., "Correlation of Optical Observations of Earth-Orbiting Objects and Initial Orbit Determination," *Presented at the 2010 AIAA/AAS Astrodynamics Specialist Conference*, AIAA Paper 2010-7975, Toronto, CA, 2010.

[11] Majji, M., Junkins, J. L., and Turner, J. D., "A High Order Method for Estimation of Dynamic Systems," *Journal of the Astronautical Sciences*, Vol. 56, No. 3, 2008, pp. 401–440.

[12] Scheeres, D. J., Han, D., and Hou, Y., "Influence of Unstable Manifolds on Orbit Uncertainty," *Journal of Guidance, Control, and Dynamics*, Vol. 24, No. 3, 2001, pp. 573–585. doi:10.2514/2.4749

[13] Scheeres, D. J., Hsiao, F.-Y., Park, R., Villac, B., and Maruskin, J. M., "Fundamental Limits on Spacecraft Orbit Uncertainty and Distribution Propagation," *Journal of Astronautical Sciences*, Vol. 54, No. 3–4, 2005, pp. 505–523.

[14] McCullaugh, P., *Tensor Methods in Statistics*, Chapman and Hall, London, 1987, pp. 24–56.

[15] Brouwer, D., "Solution of the Problem of Artificial Satellite Theory Without Drag," *Astronomical Journal*, Vol. 64, 1959, pp. 378–396.

[16] Vallado, D., *Fundamentals of Astrodyamics and Applications*, 3rd ed., Microcosm Press, Hawthorne, CA, 2007, p. 119.